KSCE Journal of Civil Engineering (2018) 22(7):2315-2324

DOI 10.1007/s12205-017-0018-y

Hydraulic Engineering

pISSN 1226-7988, eISSN 1976-3808
www.springer.com/12205

Analysis of Turbulent Flow Characteristics Around Bar using the Conditional Bursting Technique for Varying Discharge Conditions

Md. Amir Khan* and Nayan Sharma**

Received January 7, 2017/Accepted August 16, 2017/Published Online December 12, 2017

Abstract

Braided river is currently important topic of study; several scientists doing research on the complexity of braided river. However, the turbulent characteristics of flow around the braid bar is not thoroughly studied till now. In the current paper, the quadrant method is used for analyzing the turbulence characteristics of flow in the vicinity of bar using 2-D bursting events technique. Although many advances have been made within recent years in interpreting the mechanics of flow, transport of sediment and sedimentary architecture of braided rivers, many key issues remain to be addressed in particular the underlying processes of braid bar initiation. An attempt has been made herein to relate the depositional characteristics around the bar in the braided river model to the sweep and ejection bursting events. The concept of the hole is used in order to isolate the extreme events that contribute to the turbulent burst. The mean angle of sweep and ejection events possesses direct relationship with the scouring/ deposition characteristics in the vicinity of bar. The mean values contour of normalized ejection and sweep stress are plotted and their variation with the changing discharge is studied in this paper.

Keywords: *bar, turbulence, conditional shear stress, sweep/ejection events, hole size*

1. Introduction

In the natural condition, there are several river patterns such as a straight river, meandering river, braided river exist. The structure of secondary current, bed shear stress in the meandering channel have been thoroughly studied by conducting experiments and numerical simulation. Some research has been done to understand the turbulence characteristics of flow in braided river. However, these works are not sufficient to fully understand the turbulence characteristics of flow around the braid bar (Richardson and Thorne, 2001; Keshavarzi and Gheisi, 2007). Turbulent flow characteristics around the braid bar are not well researched and understood till now (Cellino and Lemmin, 2004; Czernuszenko and Rowiński, 2008).

Turbulent flow characteristics in the vicinity of bar is studied in the past. However, the association of deposition and sediment entrainment around the bar with the turbulent bursts still remains unknown. For hydraulically smooth turbulent flows, quadrant technique has been applied to determine the interactions of sediment motion and turbulent bursts (Cava *et al*., 2005). Researchers (Wu and Jiang, 2007) concluded that the shear stress did not directly related to the sediment motion but turbulent bursts (e.g. sweep, ejection) responsible for entrainment of sediment particle from the bed. Low frequency and high magnitude turbulent burst are responsible for the entrainment of sediment particle from the bed surface (Balachandar and Bhuiyan, 2007; Cuthbertson and Ervine, 2007). To fully infer the effect of turbulence on sediment motion in the vicinity of bar, the turbulent burst events required to be examined thoroughly. For shear flows over both rough and smooth beds, ejection and sweep were the main constitutive burst events in the near-bed turbulence (Keshavarzi and Gheisi, 2007; Jennifer *et al*., 2011; Khan *et al*., 2016) and ejections burst are dominated throughout the flow depth (Balachandar and Bhuiyan, 2007).

In the present study, the characteristics of the bursting phenomenon in the vicinity of bar is analyzed. Despite this importance of the bursting events in sediment transport, however, their characteristics have not been investigated in sufficient detail. As per as our knowledge, no Literature is available which relate the quadrant bursting events to the flow characteristics around the island in a braided river model.

Generally, the bar formation occurs in the falling limb of hydrograph, as the discharge decreases, the sediment carrying capacity of river also decreases, which leads to the initiation of bar formation. The bar grows downstream and in height due to the continuous deposition of sediment on its surface, diverting the water into the flanking channels, which to carry the flow, deepen and cut laterally into the original banks. Deepening of flanking channel locally lowers the water depth and the bar emerges as a bar which becomes stabilized by vegetation (Buffin-

*Research Scholar, Dept. of Water Resources Development and Management, IIT Roorkee 247667, India (Corresponding Author, E-mail: amirmdamu@gmail.com)
**Professor, Dept. of Water Resources Development and Management, IIT Roorkee 247667, India (E-mail: nayanfwt@gmail.com)

Fig. 1. Showing the Model of Braided Bar Constructed in a River Engineering Laboratory IIT Roorkee

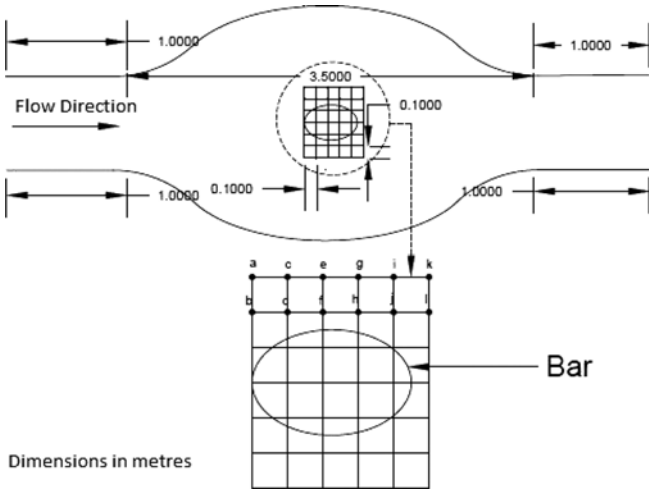

Fig. 2. Sketch of the Braided River Model

Bélanger and Roy, 2005). In recent years, many researchers had used physical based models for modeling the fluvial processes. However, limited works have been done on modeling the process of bar evolution. In the present study the flow characteristics in the vicinity of mid channel bar is studied. The experiments are performed at different discharge rate, in order to study the effect of discharge variation on the turbulent flow characteristics.

The bar model is developed using the brick and mortar. The mid bar of size 30 by 45 cm and height of 14 cm is constructed in the flume (Fig. 1). The width of channel is varying from 0.8 m to 2 m. The height of the bar is kept at 14 cm. The maximum value of channel width is taken at the center of the mid channel bar. The varying width of channel is taken in order to simulate the river bar condition. Although the size of bar has no relationship with the actual size of river bar because it is impossible to scale the actual river bar in flume. The main objective of this paper is to analyze the turbulent generated by the fluid bar interaction.

Both turbulence and stream braiding phenomena are represented by a hierarchy of scales. In turbulence the objects constituting these scales are referred as eddies; for braiding, the bar, the term is used analogously for all types of sediment bars, including the whole zoology of bar types described by the previous researchers. Turbulence and braiding both exhibit fractal behavior within the hierarchy of scales (Bergé *et al.*, 1984; Richardson and Thorne, 2001; Mazumder and Ojha, 2007; Kozioł, 2015). Also, in both types of systems interactions between structures give rise to short-lived events (ejection and sweep in turbulence and confluences in braiding) that contributes disproportionately to the overall net transport. (momentum in turbulence; sediment in braiding).

2. Experimental Program

The experiments were conducted in River Engineering Laboratory, Department of Water Resources Development and Management, Indian Institute of Technology Roorkee, India. The experiments were carried out in a flume 2.6 m wide, 1 m deep and 10 m long. Experiments were carried out at three different water flow rate of 0.06, 0.04 and 0.03 m^3/s. The tailgate was used to maintain the flow depth. The slope of the flume is kept constant for all the runs.

Velocity is measured at 12 vertical sections around the bar (as shown in Fig. 2) in a braided river model for three different discharge conditions, with the help of Acoustic Doppler Velocimetry (ADV). The detailed information of the experimental study is displayed in Table 1. For each vertical section, the velocity is measured at 10 different depths. The ADV is designed to record instantaneous velocity components at a single-point with a relatively high frequency. Measurements are performed by measuring the velocity of particles in a remote sampling volume based upon the Doppler shift effect. In most of these cases, acoustic Doppler velocimetry is the technique of choice, because it is relatively low in cost, can record at a relatively high frequency up to 100 Hz. The velocity measurements are taken at a frequency of 25 Hz in our experiment; this value is taken on the basis of fact, that the high frequency of measurement may induce spike in velocity measurement (Voulgaris and Trowbridge, 1998).

Error associated with ADV data due to spikes is removed by

Table 1. Shows the Details of Experimental Condition Performed in This Study

Serial No	Experimental Condition code	Condition	Discharge (m^3/s)	Depth of flow (cm)	Submergence Ratio
1	W	No bar	0.06	27	0.52
2	X	Presence of bar	0.06	27	0.52
2	Y	Presence of bar	0.04	23	0.61
4	Z	Presence of bar	0.03	21	0.67

Table 2. Shows the Model Experimental Results of the Scouring and Deposition Patterns at Different Positions Around Bar

Point	Experiment W Erosion/ deposition (cm)	Experiment X Erosion/ deposition (cm)	Experiment Y Erosion/ deposition (cm)	Experiment Z Erosion/ deposition (cm)
a	-1.1	-4.32	-3.42	-3.12
b	-0.91	-5.12	-4.22	-3.92
c	-0.75	-3.45	-2.55	-2.25
d	-0.82	-4.28	-2.88	-2.58
e	-0.78	-1.9	-1.6	-1.3
f	-1.21	-1.2	-1.42	-1.12
g	-1.32	0.2	0.6	1
h	-0.94	0.4	0.8	1.2
i	-0.78	0.5	0.9	1.1
j	-0.88	0.8	1.1	1.5
k	-1.12	0.9	1.2	1.6
l	-1.13	1.1	1.5	1.9

the method of (Nikora and Goring, 2000). This method is based on the concept of phase space plot where the points outside ellipsoid are defined as spikes. After detection of spikes they are replaced by interpolated values. Winadv software is used for filtering and removing the spikes from ADV data using the method of (Nikora and Goring, 2000).

The objective of this experimental program is to relate the sweep and ejection events to the deposition and erosion patterns around the bar in a braided river model. (Koken and Constantinescu, 2008) found that the sweep event is closely related to the sediment entrainment. The erosion/deposition data are collected around the bar at these selected 12 sections for three different discharge (Table 2). (Nakagawa and Nezu, 1993) found that only the extreme quadrant events contribute to the burst in turbulent flow, and in order to exclude the extreme events from low-intensity events, different sizes of a hole are defined. The average value of occurrence frequency of quadrant events is plotted for 12 different sections around the bar. The effect of hole sizes on the average value of occurrence frequency of each quadrant event is also studied in this paper. The effect of changing discharge on the turbulent characteristics of flow around the bar is also studied in this paper. The mean angle of sweep and ejection are also plotted at 12 different sections around the bar. It was found that the mean angle of sweep and ejection events are related to scouring around the bar in a braided river model. Spatial characteristics of turbulent flow is analyzed by plotting the mean value contour of normalized sweep and ejection stress at the depth of 0.6 cm. The experiments are performed for no-bar and bar conditions (Table 1). The effect of discharge variation on the spatial distribution of shear stress is also studied in this paper.

3. Methodology and Data Analysis

The recorded velocity distribution of turbulent flow is shown in Fig. 3. The conventional quadrant method involves studying the relationship between temporal fluctuations of velocity

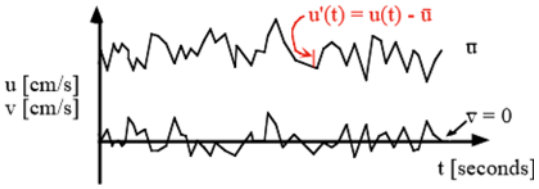

Fig. 3. Recorded Velocity Distribution for Turbulent Flow

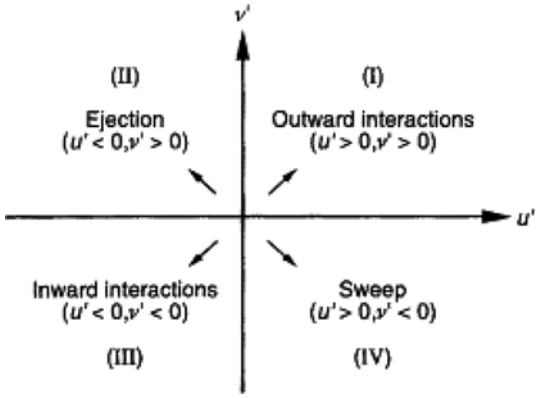

Fig. 4. Four Classes of Bursting Events and the Associated Quadrant

components, u' and v', particularly their distribution between four quadrants numbered as shown in Fig. 4. Based on quadrant analysis turbulent phenomenon is characterized into the four quadrants depending on the sign of fluctuating velocity u′ and v' (Kline *et al*., 1967).

First quadrant Outward interaction in which $u_i' > 0, v_i' > 0$

Second quadrant Ejection in which $u_i' < 0, v_i' > 0$

Third quadrant Inward interaction in which $u_i' < 0, v_i' < 0$

Fourth quadrant Sweep in which $u_i' > 0, v_i' > 0$.

Out of these four-quadrant events, sweep and ejection are relatively more important and they are related to the sediment entrainment and transport in the river. The contribution of the coherent structure mainly sweeps (Quadrant IV) and ejection (Quadrant II) are intensively studied by the several researchers (Nezu *et al*., 1994; Keshavarzi and Gheisi, 2006; Jennifer *et al*., 2011; Khan *et al*., 2016). Leopold and Wolman, 1957; Kozioł 2015; Surian, 2015 have extensively studied quadrant events, and they found that sweep is most important event that is related to transfer of momentum into the boundary layer. In addition, they found that close to bed the frequency of sweep and ejection is more as compared to the outward interaction (quadrant I) and inward interaction (quadrant III) events.

(Naot *et al.,* 1993) found that only extreme events contribute to the Reynold Stress, and the hyperbolic hole is defined in order to isolate the extreme events within each quadrant. The hole is defined by the resulting curves as yielded from Eq. (1).

$$|u'(z,t).v'(z,t)| = q\sqrt{\overline{u'(z,t)^2}}\sqrt{\overline{v'(z,t)^2}} \quad (1)$$

where q represents the hole size,the over-bar represents the time averaged value, $u'(z,t)$ and $v'(z,t)$ represent the instantaneous longitudinal and vertical turbulent fluctuations respectively.

Instantaneous Reynolds Stress for each measuring points has been filtered by applying function $E_k(z,t)$ where k = I, II, III, IV indicates the quadrant where the turbulent event falls. Discriminating function $E_k(z,t)$ has been defined below (Termini and Sammartano, 2008).

$E_I(z,t) = 1$, if $u'(z,t) > 0$; $v'(z,t) > 0$ excluding hole describe by Eq. (1) (2)

$E_I(z,t) = 0$, elsewhere

$E_{II}(z,t) = 1$, if $u'(z,t) < 0$; $v'(z,t) > 0$ excluding hole describe by Eq. (1) (3)

$E_{II}(z,t) = 0$, elsewhere

$E_{III}(z,t) = 1$, if $u'(z,t) < 0$; $v'(z,t) < 0$ excluding hole describe by Eq. (1) (4)

$E_{III}(z,t) = 0$, elsewhere

$E_{IV}(z,t) = 1$, if $u'(z,t) > 0$; $v'(z,t) < 0$ excluding hole describe by Eq. (1) (5)

$E_{IV}(z,t) = 0$, elsewhere

The function $E_k(z,t)$ shown in Eqs. (2)-(5) allows recognition of the fluctuating velocity that are contributing to the turbulent events. After excluding the turbulent event that falls in the inside region of the hole, the remaining turbulent event contributes to Reynolds stress. A small value of q leads to the selection of both strong and weak events. For the large value of hole size q only the strong events are considered for the turbulent burst. Percent occurrence of each turbulent event is calculated by Eq. (6) (Termini and Sammartano, 2008). Fig. 5 shows the structure of quadrant events for different hole sizes.

$$\left[f_K(z) = \frac{\sum_{t=0}^{T} E_k(z,t)}{\sum_{t=0}^{T} E_I(z,t) + \sum_{t=0}^{T} E_{II}(z,t) + \sum_{t=0}^{T} E_{III}(z,t) + \sum_{t=0}^{T} E_{IV}(z,t)} \right] \quad (6)$$

where $\sum_{t=0}^{T} E_k(z,t)$ is the number of turbulent event occurring in the k-th quadrant excluding hole, T is the measurement time length.

Table 2 shows the experimental results of scouring and deposition patterns at 12 points around the bar in a braided river model for three different experimental conditions. The bed levels at these points were taken before starting and after completion of the experiments. The differences between the final bed level after the completion of experiments and the initial bed level were calculated, wherein negative values of difference represent the erosion and positive values represent the deposition at that points.

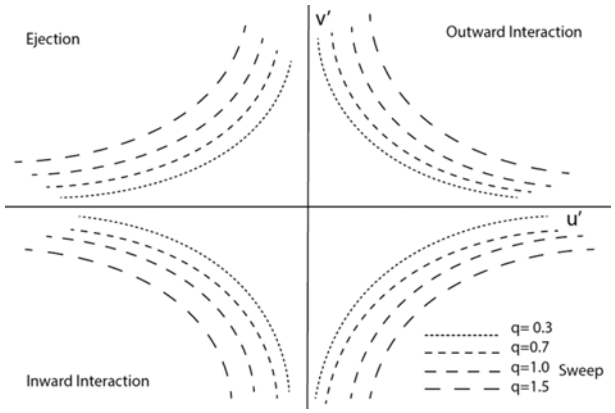

Fig. 5. Shows the Quadrant Event for Different Hole Size

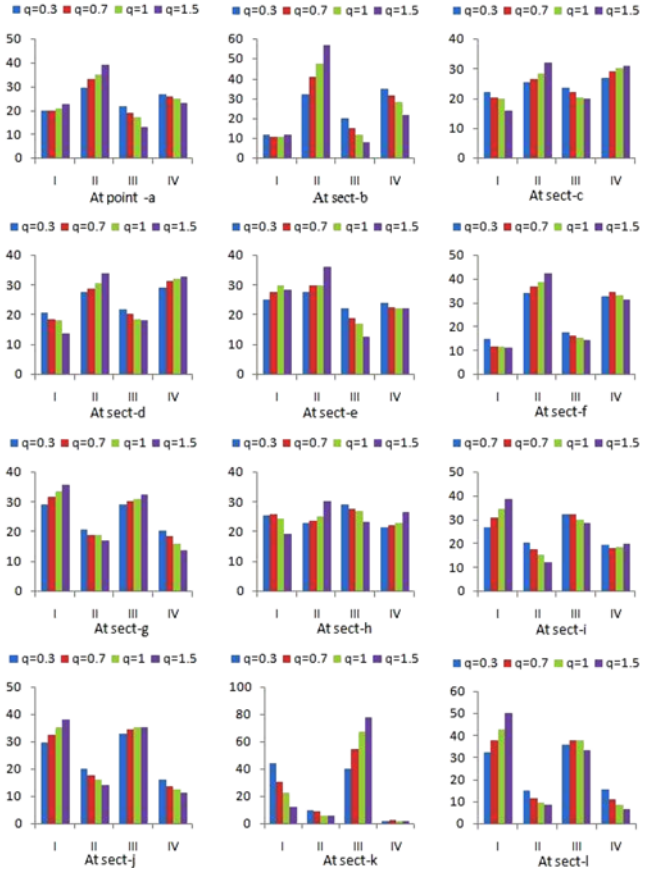

Fig. 6. The Histogram of the Values of $f_K(z)$ Determined at a Depth of 0.6 cm from the Bed for Four Different Threshold Level (q = 0.3, q = 0.7,q = 1, q =1 .5) at 12 Point Near the Braided Bar (experimental condition X)

The histogram of occurrence frequency of each quadrant events for different sizes of hole and discharge at 12 vertical sections are displayed in (Figs. 6, 7 and 8). The occurrence frequency of quadrant events for the experimental conditions X (Fig. 6), shows that the sweep and ejection are dominant events from point 'a' to point 'f'. The outward interaction and inward interaction are dominant events at the remaining six points. The occurrence frequency of each quadrant events is plotted for different values of hole size. At point 'a', the dominant events are ejection, frequency of ejection events is around 31% at q = 0.3, it is increased to 41% at q = 1.5. Similarly, the occurrence frequency of outward interaction (dominating events) at point 'g' increases from 29.24 at q = 0.3 to 36.14 at q = 1.5 (Fig. 6). From above results, it is clearly visible that the occurrence frequency of the dominant events increases with increase in the size of the hole. The main function of the hole is to filter out the extreme event from the low magnitude event. The hole filtered out the extreme events that are contributing to the burst. Table 2 shows that the

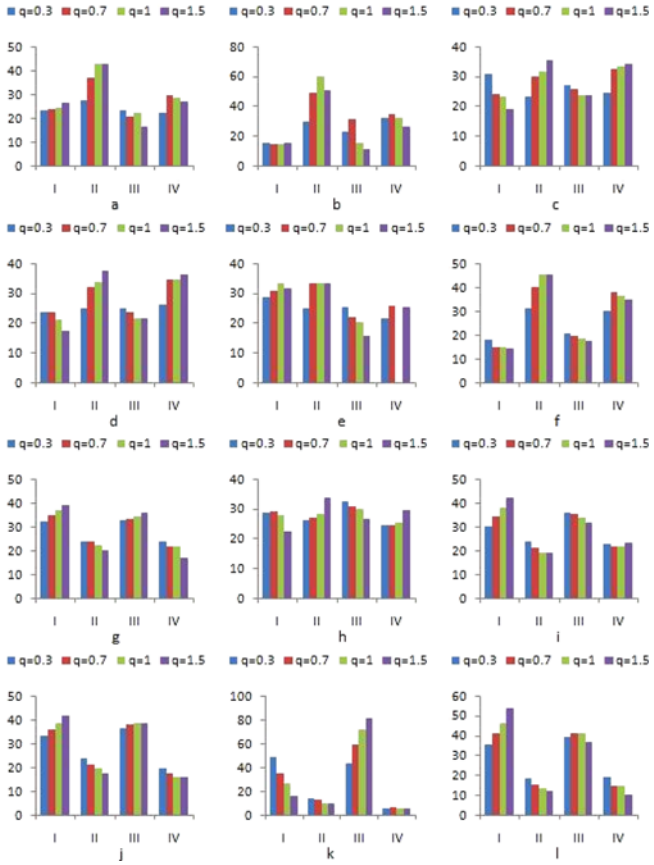

Fig. 7. The Histogram of the Values of $f_K(z)$ Determined at a Depth of 0.6 cm from the Bed for Four Different Threshold Level (q = 0.3, q = 0.7, q = 1, q = 1.5) at 12 Point Near the Braided Bar (experimental condition Y)

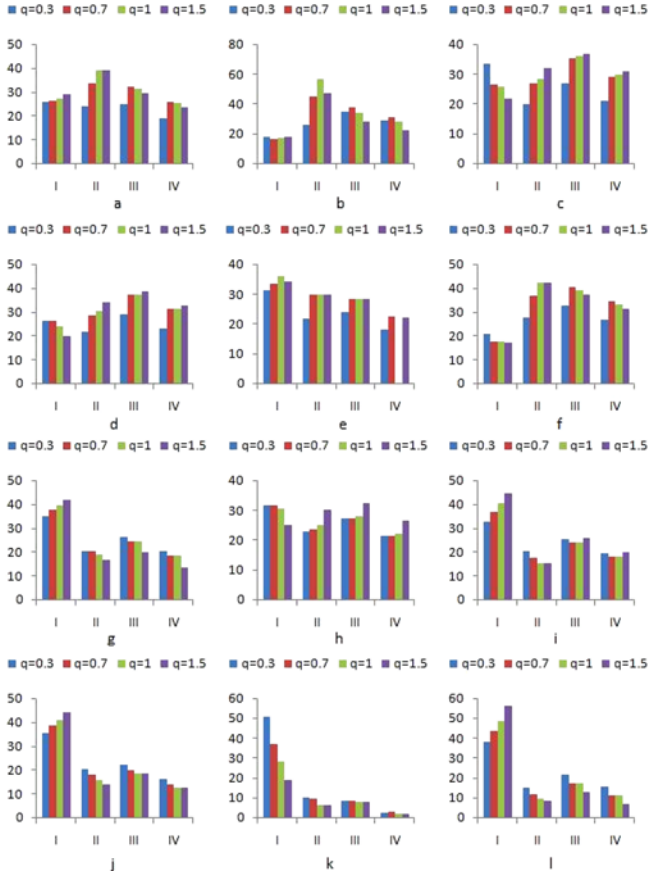

Fig. 8. The Histogram of the Values of $f_K(z)$ Determined at a Depth of 0.6 cm from the Bed for four Different Threshold Level (q = 0.3, q = 0.7,q = 1, q = 1.5) at 12 Point Near the Braided bar (experimental condition Z)

scouring occurs at sections 'a' to 'f' and depositions occurs at the remaining six sections. After analysis of the occurrence frequency of each quadrant events (Fig. 6), it was found that the even events are dominant at scouring sections, and odd events are dominant at depositional sections. Thus, it can be concluded that 'sweep' and 'ejection' events are related to erosion. Evidently, higher values of sweep and ejection occurrence frequency indicate the erosion, whereas 'outward interaction', and 'inward interaction' events are dominant at depositional points.

Experiments were performed at three different discharge conditions, in order to study the effect of changing discharge on the turbulent characteristics of flow around the bar. For the hole size of 0.3, the average occurrence frequency of the sweep events at point 'a' decreases from 30.15 to 27.15 when the discharge decreases from 0.06 to 0.05 cm^3/s, the average occurrence frequency of sweep events is further decreased to 24.15 at the discharge of 0.03 cm^3/s (Figs. 6 to 8). The average occurrence frequency of ejection events shows the similar trend with the discharge. Remaining 11 points also shows the similar decrease in occurrence frequency of sweep and ejection events with a decrease in the value of discharge. As stated earlier above, scouring and deposition pattern around a bar in a braided river model is presented in Table 2, which shows that the deposition occurs at the points 'g', 'h', 'i', 'j', 'k', 'l', and the deposition at these points increases with the decrease in discharge. So from the above results, it can be concluded that the average occurrence frequency of sweep and ejection decreases and deposition around the bar increases with a decrease in the discharge. The above observations show that the occurrence frequency of sweep and ejection events are inversely related to deposition around the bar in the braided river model.

3.1 The Angle of the Events

The applied force on the bed particles depends on the inclination angle of the force. The angle of a particular event is defined as the angle of turbulent velocity vector with respect to the longitudinal axis. The angle of an event is determined using Eq. (7) (Keshavarzi and Gheisi, 2006).

$$\theta_{sweep} = arctan\left(\left|\frac{v'_{sweep}}{u'_{sweep}}\right|\right), \theta_{ejection} = arctan\left(\left|\frac{v'_{ejection}}{u'_{ejection}}\right|\right) \quad (7)$$

u'_{sweep}, v'_{sweep} are obtained using the post processing of velocity data. First of all, turbulent fluctuations u', v' are computed by subtracting the velocity values from their mean value.

Mean velocity $\bar{u} = \frac{1}{N}\sum_{1}^{N} u_i$

Turbulent fluctuation = $u_i' = u_i = \bar{u}$

Here, N is total number of velocity sample, u_i is instantaneous value of velocity, $\bar{u}$ is mean value of N velocity samples and u_i' is instantaneous turbulent fluctuation of i[th] velocity sample. Similarly, the v_i' is computed. The u_i' and v_i' are decomposed on the basis of their quadrant. Thus the u'_{sweep} indicate the longitudinal velocity fluctuation for sweep quadrant and v'_{sweep} indicate the vertical velocity fluctuation for sweep quadrant.

where $\theta_{sweep}, \theta_{ejection}$ are the angle of sweep and ejection events measured from the horizontal axis.

The magnitude of the mean angle of events for sweep and ejection events are different and it is not acceptable. In order to compute the mean values of sweep and ejection events, the data are transformed into normal distribution using the Box–Cox power transformation.

The values of the mean angle for sweep and ejection events can be computed by averaging the temporal values of sweep and ejection angle. However, the temporal values of sweep and ejection events are not uniformly distributed and thus their mean values do not represent the actual mean sweep and ejection angle. In order to compute the actual mean values of sweep and ejection events, the data are transformed into normal distribution using the Box–Cox power transformation. A Box-Cox power transformation transformed the original data qi to the transformed data denoted by $B(\theta_i)$. Here θ_i represents the temporal values of angle of events of i[th] quadrants, for ejection events $i = 2$ and $i = 4$ for sweep events.

A Box-Cox power transformation is defined, for non-zero values of λ given by Eq. (8).

$$B(\theta_i) = \frac{(\theta_i + k)^{\lambda} - 1}{\lambda} \tag{8}$$

and, for zero value of λ, by Eq. (9).

$$B(\theta_i) = \ln(\theta_i + k) \tag{9}$$

In the above equations, k is a constant and λ is transformation power. If all the values of anele of events, θ are greater than zero then the value of constant k is taken as zero. Box-Cox transformation is applied to a dataset which comprises quadrant IV events (sweep events) and quadrant II events (ejection events). The inverse transformation B^{-1} of $B(\theta_i)$ for this situation is given by Eq. (10).

$$\theta = [\lambda B(\theta_i) + 1]^{\frac{1}{\lambda}} \tag{10}$$

The mean values of transformed angle of events for sweep and ejection quadrants were calculated using Eqs. (11).

$$\left(\overline{B(\theta)_i} = \frac{1}{n}\sum_{i=1}^{n} B(\theta_i)\right)_{i=2,4} \tag{11}$$

The inverse Box-Cox transformation was applied to these mean values of sweep and ejection events to enable determination of the mean angle of sweep and ejection events.

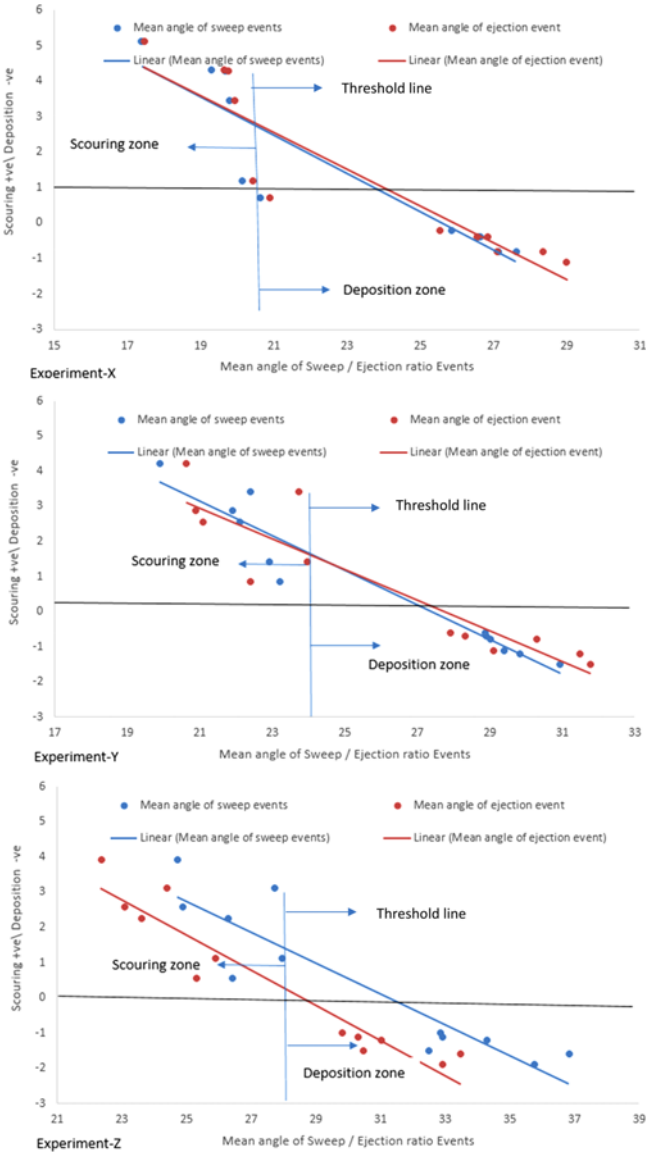

Fig. 9. Shows the Angle of Sweep and Ejection Events and Scouring/deposition Pattern Plotted at 12 Points Around the Island in a Braided River Model for Three Different Experimental Conditions

Figure 9 shows the relationships of mean angle of sweep, ejection events with the erosion/deposition magnitude at 12 vertical sections around the bar, for three different experimental conditions. Threshold lines is also displayed in Fig. 9, this line divides the erosion and deposition area on the basis of mean value of sweep and ejection angle, the values of mean angle of sweep and ejection events greater than the threshold value lies under the deposition zone and vice versa. For each discharge condition, the sweep/ejection ratio shows linear relationship with the erosion/deposition magnitude. The above discussions show that the mean angle of sweep and ejection are strongly related with the erosion/deposition magnitude around the bar in a braided river model.

The main reason for performing this part for three different experimental conditions, is to study the effect of varying discharge on the mean angle parameters and thresholds value. The values of threshold are 20.5,24,28 degrees for experimental conditions X, Y, Z respectively, the value of threshold increases with decrease in discharge values. At point 'a', the value of an angle of sweep events increases from 19.3 to 22.4 when the discharge decreases from 0.06 m^3/sec to 0.05 m^3/sec (Fig. 9). A similar increase in angle of sweep and ejection event occurs for remaining 11 points. The results show that the mean sweep/ ejection angle and threshold value increases with decrease in the discharge.

3.2 Conditional Shear Stress

The mean quadrant shear stresses differ from the temporal mean shear stress. (Nezu *et al.*, 1994) found that the sweep and ejection stresses are primarily responsible for sediment entrainment and deposition. In order to study the sweep and ejection stresses effect on erosion/deposition characteristics, normalized sweep and ejection stress parameters are defined. The instantaneous values of sweep and ejection stress are normalized by the total mean shear stress. The new parameters, normalized sweep and ejection stress are defined in this paper (Eq. (12)).

$$\tau_{nes} = \frac{\tau_e}{\bar{\tau}},\ \tau_{ness} = \frac{\tau_s}{\bar{\tau}} \tag{12}$$

In the above equation, τ_e, τ_s are the instantaneous sweep and ejection stress respectively and $\bar{\tau}$ is the total mean shear stress at that point in the flow. τ_{ness}, τ_{ness} are the normalized sweep and ejection stress respectively. The total stress is computed using the formula, Reynolds stress = $\rho u_i' v_i'$. The product of the fluctuating velocity component $u_i' v_i'$ is decomposed into the four parts, on the basis of the fluctuating velocity signs.

The sweep stress is the average value of $\rho u_i' v_i'$ for which $u_i' > 0$, $v_i' < 0$. Similarly, the ejection stress is computed.

For transforming the sweep and ejection stress data into the normal distribution, box cox transformation is used. Frequency distribution of the transformed values of τ_{nes}, τ_{nss} are shown in Fig. 10(a), (b) respectively. The transformed ejection and sweep shear stress data follows the Gaussian distribution. The normal probability plot of transformed ejection and sweep shear stress data are shown in Fig. 11(a), (b) respectively. The value of correlation coefficient for τ_{nes}, τ_{nss} were found to be 0.98 and 0.99 respectively. The critical correlation coefficients for acceptance of the normality hypothesis with a 0.05 level of significance are 0.94 and 0.96 for τ_{nes} and τ_{nss} respectively. These critical values are less than correlation coefficient for τ_{nes} and τ_{nss}, thus the Box-

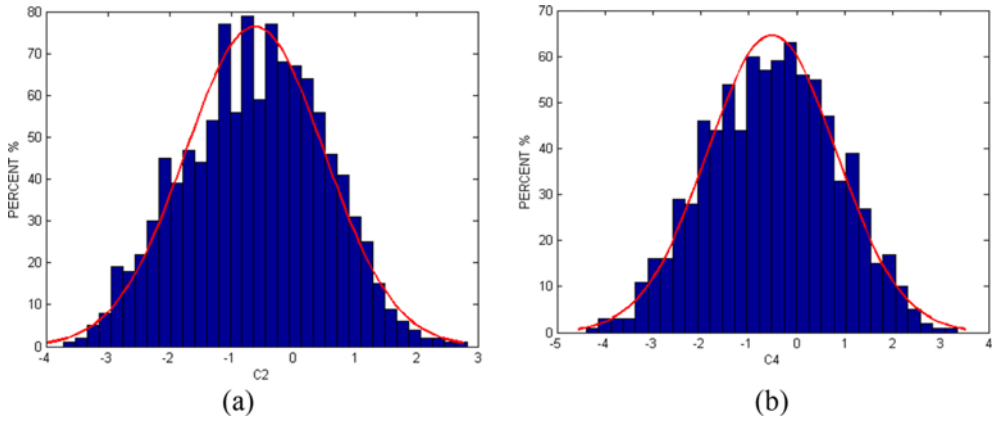

Fig. 10. (a, b) Shows the Frequency Distributions of the Transformed Data of Normalized Ejection and Sweep Shear Stress Respectively

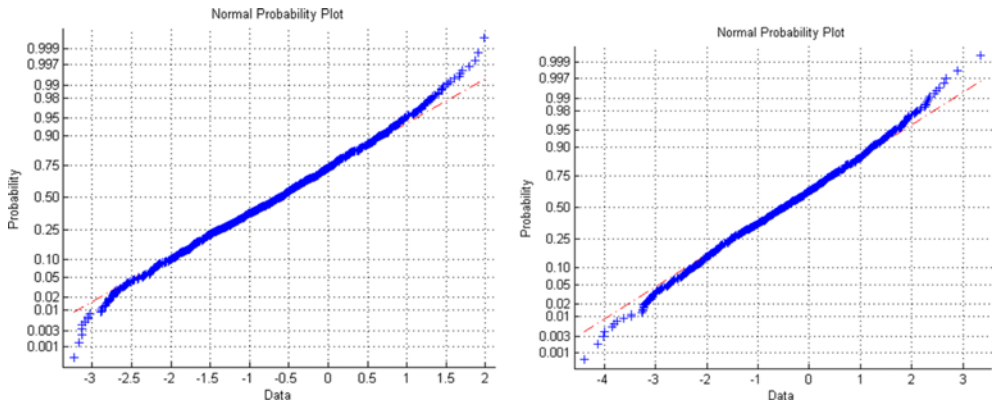

Fig. 11. (a, b) Shows the Probability Distributions of the Transformed Sweep and Ejection Shear Stress Respectively

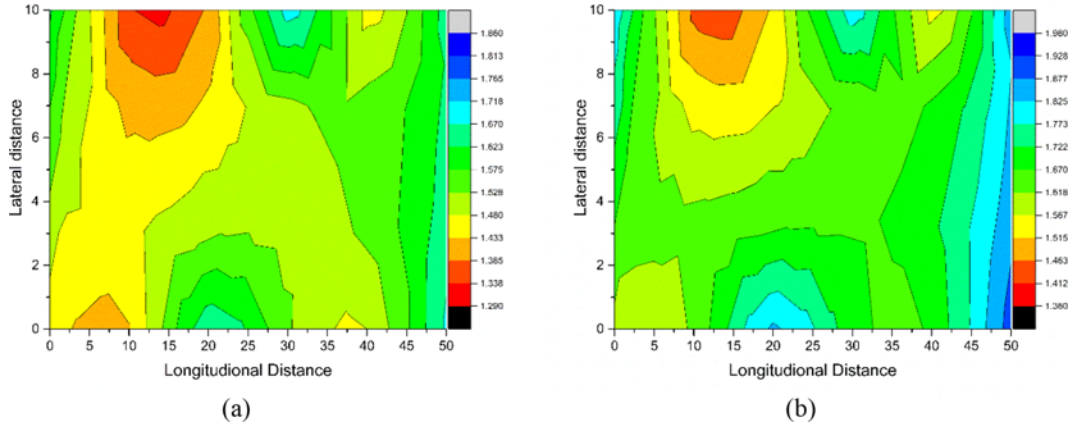

Fig. 12. (a, b) Shows the Mean Value of Normalized Ejection and Sweep Stress Respectively for no Bar Condition

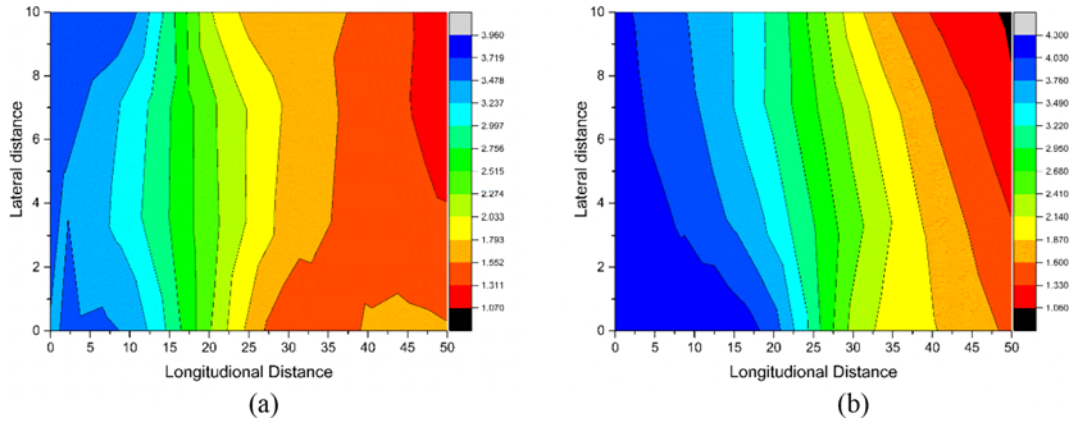

Fig. 13. (a, b) Shows the Mean Value of Normalized Ejection and Sweep Stress Respectively for Experimental Condition X

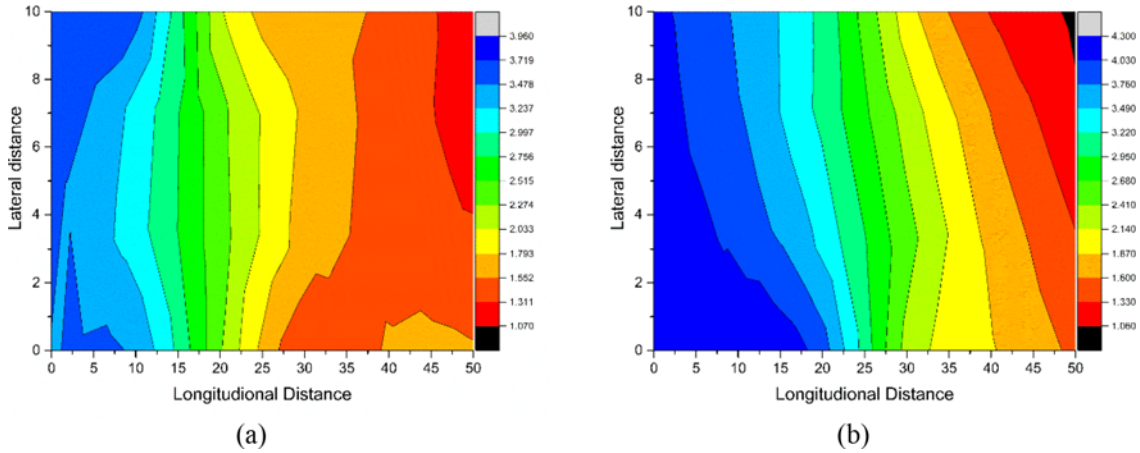

Fig. 14. (a, b) Shows the Mean Value of Normalized Ejection and Sweep Stress Respectively for Experimental Condition Y

Cox method is effective for transforming the shear stress data into the normal distribution.

The mean value of normalized sweep and ejection shear stress are obtained by using the Eqs. (8) to (11) as described in the previous section. In order to study the spatial distribution of shear stress around the bar, the mean values contour of τ_{nes}, τ_{nss} are plotted at the depth of 0.6 cm, for four different experimental conditions (Table 2). For experimental condition W (no bar condition), the mean value of τ_{nes} and τ_{nss} are nearly uniform, lies between 1.2 to 1.9 (Fig. 12). Table 2 shows that the scouring occurs at all 12 locations, for no bar condition. Uniform characteristics of τ_{nes} and τ_{nss} contour indicate that the flow is not feasible for entrainment and transportation of sediment particle, which is also indicated in Table 2, as the value of scouring is much less as compared to the other experimental conditions. For the experimental condition X, the mean value of τ_{nes} and τ_{nss}

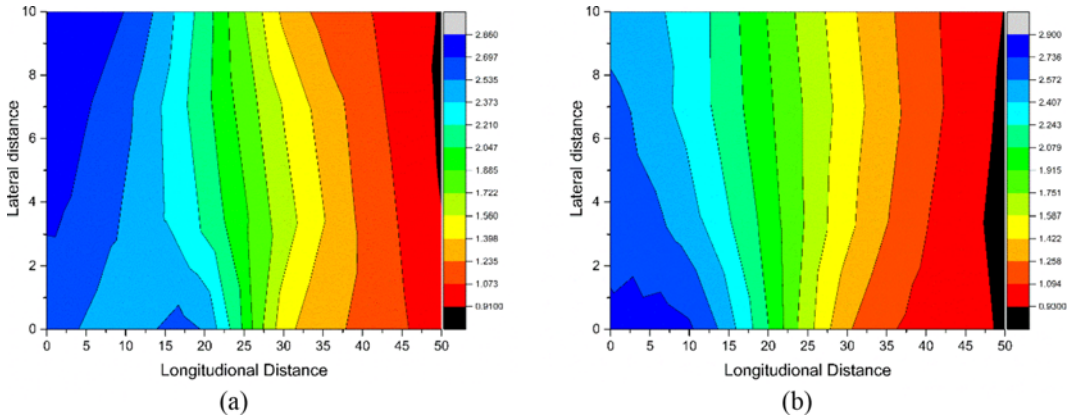

Fig. 15. (a, b) Shows the Mean Value of Normalized Ejection and Sweep Stress Respectively for Experimental Condition Z

contour value lies between 1 and 4 (Fig. 13). Table 2 show that the scouring occurs for the first 25 cm longitudinal distance and deposition occurs for the remaining 25 cm longitudinal distance (For Experimental Condition X). As shown in Fig. 13, the mean value of τ_{nes} and τ_{nss} are quite less for the last 25 cm longitudinal distance as compared to the first 25 cm distance. The high values of τ_{nes} and τ_{nss} contours for the first 25 cm, indicate the effect of sweep and ejection stress on the sediment entrainment, this results is in accordance with the previous researches. For experimental condition Y (Fig. 14), the maximum value of τ_{nes} and τ_{nss} contours are 2.8 and 2.9 respectively, these values are much lesser as compared to their corresponding values for experimental condition X. Table 2 shows that the scouring value occurs at sections 'a' to 'f' for experimental conditions Y are much less than the corresponding values for experimental condition X. The above results shows that the τ_{nes} and τ_{nss} contours values decreases significantly as the value of discharge decreases, this indicate that at lower discharge, the sweep and ejection shear stress are less competence for sediment entrainment and transportation. For the experimental condition Z (Fig. 15), the minimum value of τ_{nes} and τ_{nss} contours are 0.79 and 0.91 respectively, these low values occurs for depositional area. The lower values of τ_{nes} and τ_{nss} (lesser than unity) at depositional area indicate the dominance of outward and inward interaction at the depositional area.

4. Results and Discussions

Turbulent flow characteristics around the bar are analysed with the help of quadrant technique. Conditional analysis is done by plotting the occurrence frequency of bursting events for different hole size. Special attention has been given to sweep and ejection events, as they are responsible for entrainment and transportation of sediment. Average value of angle of events for 12 vertical sections are plotted against the scouring/deposition values at these sections. The results show the positive linear correlation between them. The sweep and ejection stress contours are plotted for studying the spatial distribution of turbulent flow around the bar. From the analysis, it was found that these sweep and ejection shear stress values are closely related with the scouring/depositional characteristics.

5. Conclusions

1. The experimental results show that the occurrence frequency of the sweep and ejection events are related to erosion around the bar in the braided river model, and the occurrence frequency of the outward interaction and inward interaction are related to the deposition. The occurrence frequency of sweep and ejection events decreases with the decrease in discharge, this leads to increase in deposition around the bar. After studying the histogram of quadrant analysis, it was found that dominating quadrant events become more dominant at a higher value of hole size.
2. Threshold value of mean angle of sweep/ejection are computed for three different experimental conditions. The effect of discharge variation on mean sweep and ejection angle are studied in this paper. The threshold value of sweep/ejection events decreases with the increase in discharge. The results show that the sweep and ejection angle are important parameters, as they are linearly related with the erosion/deposition magnitude around the bar in a braided river model.
3. In order to study the sweep and ejection stresses effect on erosion/deposition characteristics, the new parameters, normalized sweep and ejection stress are defined in this paper. The results shows that the τ_{nes} and τ_{nss} contours values decreases significantly as the value of discharge decreases, this indicate that at the lower discharge, the sweep and ejection shear stress are less competence for sediment entrainment and transportation. For the experimental condition Z, the minimum value of τ_{nes} and τ_{nss} contours are 0.79 and 0.91 respectively, these low values occurs for depositional area. The lower values of τ_{nes} and τ_{nss} (lesser than unity) at depositional area indicate the dominance of outward and inward interaction at the depositional area.

References

Balachandar, R. and Bhuiyan, F. (2007). "Higher-order moments of

velocity fluctuations in an open-channel flow with large bottom roughness." *Journal of Hydraulic Engineering*, Vol. 133, No. 1, pp. 77-87, DOI: 10.1061/(ASCE)0733-9429(2007)133:1(77).

Bergé, P., Pomeau, Y., and Vidal, C. (1984). *Order within chaos,* Wiley and Sons NY, DOI: 10.1002/bbpc.198800028.

Buffin-Bélanger, T. and Roy, A. G. (2005). "1 min in the life of a river: Selecting the optimal record length for the measurement of turbulence in fluvial boundary layers." Geomorphology, Vol. 68, No. 1, pp. 77-94.

Cava, D., Schipa, S., and Giostra, U. (2005). "Investigation of low-frequency perturbations induced by a steep obstacle." *Boundary-layer Meteorology*, Vol. 115, No. 1, pp. 27-45, DOI: 10.1007/s10546-004-2123-y.

Cellino, M. and U. Lemmin (2004). "Influence of coherent flow structures on the dynamics of suspended sediment transport in open-channel flow." *Journal of Hydraulic Engineering*, Vol. 130, No. 11, pp. 1077-1088.

Cuthbertson, A. and Ervine, D. (2007). "Experimental study of fine sand particle settling in turbulent open channel flows over rough porous beds." *Journal of Hydraulic Engineering,* Vol. 133, No. 8, pp. 905-916, DOI: 10.1061/(ASCE)0733-9429(2007)133:8(905).

Czernuszenko, W. and Rowiński, P. (2008). "Shear stress statistics in a compound channel flow." *Arch Hydro-Engin Environ Mech*, Vol. 55, Nos. 1-2, pp. 3-27.

Jennifer, D., Li, H., Guangqian, W., and Xudong, F. (2011). "Turbulent burst around experimental spur dike." *International Journal of Sediment Research,* Vol. 26, No. 4, pp. 471-523, DOI: 10.1061/41114(371)179.

Keshavarzi, A. and Gheisi, A. (2007). "Three-dimensional fractal scaling of bursting events and their transition probability near the bed of vortex chamber." *Chaos, Solitons & Fractals*, Vol. 33, No. 2, pp. 342-357, DOI: 10.1016/j.chaos.2006.01.020.

Keshavarzi, A. R. and Gheisi, A. R. (2006). "Stochastic nature of three dimensional bursting events and sediment entrainment in vortex chamber." *Stochastic Environmental Research and Risk Assessment*, Vol. 21, No. 1, pp. 75-87, DOI: 10.1007/s00477-006-0045-6.

Khan, M. A., Sharma, N., and Singhal, G. D. (2016). "Experimental study on bursting events around a bar in physical model of a braided channel." *ISH Journal of Hydraulic Engineering*, pp. 1-8, DOI: 10.1080/09715010.2016.1239554.

Kline, S., Reynolds, W., Schraub, F., and Runstadler, P. (1967). "The structure of turbulent boundary layers." *J. Fluid Mech*, Vol. 30, No. 4, pp. 741-773.

Koken, M. and Constantinescu, G. (2008). "An investigation of the flow and scour mechanisms around isolated spur dikes in a shallow open channel: 2. Conditions corresponding to the final stages of the erosion and deposition process." *Water Resources Research*, Vol. 44, No. 8, DOI: 10.1029/2007WR006491.

Kozioł, A. (2015). "Scales of turbulent eddies in a compound channel." *Acta Geophysica,* Vol. 63, No. 2, pp. 514-532, DOI: 10.2478/s11600-014-0247-0.

Leopold, L. and Wolman, M. (1957). *River channel patterns,* Fluv Geom: Geom Crit Conc Vol: 3.

Mazumder, B. and Ojha, S. P. (2007). "Turbulence statistics of flow due to wave–current interaction." *Flow Measurement and Instrumentation*, Vol. 18, No. 3, pp. 129-138, DOI: 10.1029/2008JF001203.

Naot, D., Nezu, I., and Nakagawa, H. (1993). "Hydrodynamic behavior of compound rectangular open channels." *Journal of Hydraulic Engineering*, Vol. 119, No. 3, pp. 390-408, DOI: 10.1061/(ASCE)0733-9429(1994)120:7(892.2).

Nezu, I., Nakagawa, H., and Jirka, G. H. (1994). "Turbulence in open-channel flows." *Journal of Hydraulic Engineering*, Vol. 120, No. 10, pp. 1235-1237, DOI: 10.1017/S0022112094211618.

Nikora, V. and Goring, D. (2000). "Flow turbulence over fixed and weakly mobile gravel beds." *Journal of Hydraulic Engineering*, Vol. 126, No. 9, pp. 679-690, DOI: 10.1061/(ASCE)0733-9429(2000)126:9(679).

Richardson, W. R. and Thorne, C. R. (2001). "Multiple thread flow and channel bifurcation in a braided river: Brahmaputra–Jamuna River, Bangladesh." *Geomorphology*, Vol. 38, No. 3, pp. 185-196, DOI: 10.1016/S0169-555X(00)00080-5.

Surian, N. (2015). *Fluvial Processes in Braided Rivers,* Rivers–Physical, Fluvial and Environmental Processes, Springer: 403-425, DOI: 10.1007/978-3-319-17719-9_15.

Termini, D. and Sammartano, V. (2008). "Experimental analysis of relations between coherent turbulent structures and formation of bedforms." *Arch Hydro-Eng Environ Mech.*, Vol. 55, Nos. 3-4, pp. 125-143.

Voulgaris, G. and Trowbridge, J. H. (1998). "Evaluation of the Acoustic Doppler Velocimeter (ADV) for turbulence measurements*." *Journal of Atmospheric and Oceanic Technology,* Vol. 15, No. 1, pp. 272-289.

Wu, F.-C. and Jiang, M.-R. (2007). "Numerical investigation of the role of turbulent bursting in sediment entrainment." *Journal of Hydraulic Engineering,* Vol. 133, No. 3, pp. 329-334, DOI: 10.1061/(ASCE)0733-9429(2007)133:3(329).